Fluid Dynamics Assessment of the Tesla Turbine Rotor

Giampaolo Manfrida[a], Lorenzo Talluri[b]

[a] Dipartimento di Ingegneria Industriale,Università di Firenze, Firenze, Italy, giampaolo.manfrida@unifi.it
[b] Dipartimento di Ingegneria Industriale,Università di Firenze, Firenze, Italy, lorenzo.talluri@unifi.it

Abstract:

The Tesla turbine seems to offer several points of attractiveness when applied to low-power applications. Indeed, it is a simple, reliable, and low cost machine. The principle of operation of the turbine relies on the exchange of momentum due to the shear forces originated by the flow of the fluid through a tight gap among closely stacked disks.

The Tesla turbine did not raise much interest when Tesla first spread his idea; in recent years, as micro power generation gained attention on the energy market place, this original expander raised renewed interest.

The mathematical model of the Tesla turbine rotor is revised in this paper, and adapted to real gas operation. The model is first validated by comparison with other assessed literature models. The optimal configuration of the rotor geometry is then investigated running a parametric analysis of the fundamental design parameters. High values of efficiency (isolated rotor) were obtained for the optimal configuration of the turbine, which appears interesting for small-scale power generation. The rotor efficiency depends on the configuration of the disks, particularly on the gap and on the outlet diameter, which determines largely the kinetic energy at discharge.

Finally, the expander is located on the Balje diagram and it is found to be potentially competitive with volumetric expanders or drag turbines.

Keywords:

Tesla Turbine, Expander, Rotor.

1. Micro generation and the Tesla Turbine

In recent years, distributed micro generation of power has become of paramount consideration by industries, governments and research institutions.

One of the main problems of micro generation of power in thermal energy conversion applications is related to the expander, as this component often presents high manufacturing costs and low reliability. The Tesla turbine seems to tackle these problems. Its simple structure ensures a very reliable and low-cost machine.

The Tesla turbine was first patented by Tesla in 1913 [1]. The first description of the bladeless turbine was given in the patent (Figure 1). It can be described as a multiple parallel flat rigid disks assembly connected to a rotating shaft. The disks are arranged co-axially in order to maintain a very small gap between them. The radial-inflow admission of the working fluid is from one or more tangential nozzles, providing a strong tangential component. The working fluid moves from the inlet to the outlet radius due to the difference in pressure determined by friction and by the exchange of momentum, and exits from openings made on the disks and/or shaft at the inner radius.

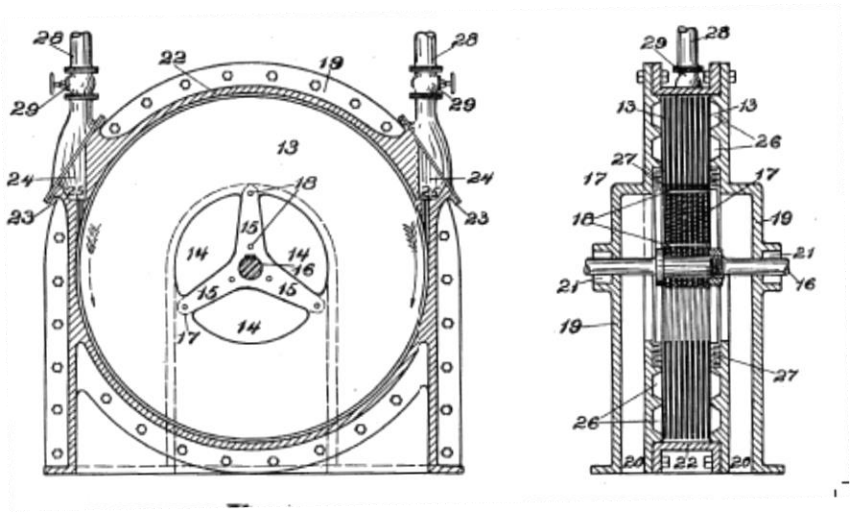

Fig. 1 – Figures from Tesla's Patent, 1913 [1]

The Tesla turbine did not encounter much success when it was proposed, and eventually it was not investigated deeply and further developed for a long time.

Only in the 1950s Armstrong was built an experimental test rig to investigate the performance of the disk turbine [2]. He conducted a test campaign, with steam as working fluid and different nozzle configurations. A valuable result was the understanding of one of the causes of inefficiency. Indeed, it was found that the nozzle flow strongly affects the performance of the turbine.

After the Armstrong tests the Tesla turbine was not investigated for another 15 years. Only with Rice [3], a sound analytic/numerical model, based on the physics of the flow, was developed. The radial velocity rises proceeding towards the centre due to the reduction of the flow area. The tangential velocity is determined by the local balance of the force components (momentum/friction). The mathematical model performed a notable simplification of the Navier-Stokes equations, allowing tackling the solution with the first computers available at the time. The main assumptions were to consider steady flow of an inviscid incompressible working fluid.

Rice built and tested 6 different types of disk turbines, with air as working fluid. The first turbine was carefully built following Tesla's patent indications. The results of his work demonstrated the feasibility of the multiple-disk turbine for low-power application. On the other hand, he also found that the Tesla turbine would not be competitive with conventional turbines for medium to high power application, mainly because the sum of several losses (non-isentropic expansion in the nozzles, uncontrolled diffusion at the outlet of the rotor, bearing and seal losses…) increases with the power output.

After Rice's pioneer work, research on the Tesla turbine was set aside until recent times. Lately, new research has flourished on the subject.

Hoya and Guha [4] designed and built a new test rig for measuring the output torque and power of a Tesla turbine. In a following work [5], Guha investigated the nozzle recognizing it as the source of the major irreversibility according to their test results; he demonstrates that a careful design of the nozzle could reduce the nozzle losses by 40-50 %. Also Neckel and Godinho [6] focused their research on nozzle geometry. In their research 10 nozzles were designed, manufactured and tested with air as working fluid. Their study confirmed that the nozzle is the critical component of the turbine and that an adequate design could contribute to increase the overall efficiency of the turbine.

Carey [7] presented an assessment of the disc turbine for a small-scale application. He developed an analytical solution of the governing equations, declaring an achievable isentropic efficiency of 75% in optimal design conditions. A complete computational and theoretical modelling of the flow

inside a Tesla turbine was presented by Carey [8]. In this work, he fully explains the advantages and drawbacks of computational and analytical analysis. Furthermore, Carey also discusses the advantages of using this expander for green-energy applications. Guha and Sengupta [9, 10] developed an accurate fluid dynamics model of the turbine, analyzing individually the role of each force (centrifugal, Coriolis, inertial and viscous). Lemma et al. and Guha and Sengupta [11, 12], also developed a CFD analysis and a general characterization of the performance of the Tesla turbine.

The development of a micro Tesla turbine was investigated by Romanin et al. [13]. In this study, the experimental data showed that a 1 cm rotor could achieve an efficiency of 36 %. Starting from these data, Krishan et al. developed scaling laws and gave recommendations for the development of a 1 mm Tesla turbine [14]. Guha and Sengupta also developed a similitude study on the flow of the Tesla turbine [15]. The scaling laws were obtained through the use of Bucking Pi theorem, which lead to the definition of 7 fundamental non-dimensional numbers. A further study of Guha and Sengupta [16] demonstrated that the application of the Euler turbomachinery equation is consistent only if local velocity mass-averaged values are considered. Recent published work on the Tesla turbine deals with the investigation of nanofluids applications [17]; an increase of power output of 30% appears to be possible when the volume fraction of nanoparticles increases from 0 to 0.05.

There have been several interesting studies undertaken on experimental test rigs on the Tesla turbine and on the development of its mathematical model. However, there still exists a literature gap on the fluid dynamics optimization analysis of the rotor for compressible fluids, as well as for real-fluid effects which are likely using refrigerants or advanced working fluids already utilized for low-power and low-temperature applications.

Therefore, the principal aim of this study is to build a mathematical model of the rotor in order to assess the optimum geometry, as well as to assemble a numerical tool to evaluate the performance of the Tesla turbine.

Another objective is to set the machine on the Balje diagram in order to understand to which technologies it can be compared.

2 Model of the Rotor Flow

2.1 General Flow Equations and assumptions

The model for the rotor flow is derived from [3, 7, 9] with some notable changes:

- The hypothesis of incompressible flow with constant density is removed;
- Density – as well as all other thermodynamic functions – is taken as a fluid property depending on the local variables (typically, pressure and temperature);
- A real fluid model is applied (no perfect gas assumptions).

Because of these assumptions, the equations are solved numerically with fluid properties locally evaluated by EES. In the following, the fundamental Navier-Stokes equations in cylindrical coordinates are briefly recalled:

Continuity:

$$\frac{1}{r}\frac{\partial(r\rho V_r)}{\partial r}+\frac{1}{r}\frac{\partial(\rho V_\theta)}{\partial \theta}+\frac{\partial(\rho V_z)}{\partial z}+\frac{\partial \rho}{\partial t}=0 \quad (1)$$

Momentum, r-direction:

$$V_r\frac{\partial V_r}{\partial r}+\frac{V_\theta}{r}\frac{\partial V_r}{\partial \theta}+V_z\frac{\partial V_r}{\partial z}-\frac{{V_\theta}^2}{r}=-\frac{1}{\rho}\left(\frac{\partial p}{\partial r}\right)+\nu\left\{\frac{1}{r}\frac{\partial}{\partial r}\left(r\frac{\partial V_r}{\partial r}\right)+\frac{1}{r^2}\frac{\partial^2 V_r}{\partial \theta^2}+\frac{\partial^2 V_r}{\partial z^2}-\frac{V_r}{r^2}-\frac{2}{r^2}\frac{\partial V_\theta}{\partial \theta}\right\}+f_r \quad (2)$$

Momentum, θ-direction:

$$V_r\frac{\partial V_\theta}{\partial r}+\frac{V_\theta}{r}\frac{\partial V_\theta}{\partial \theta}+V_z\frac{\partial V_\theta}{\partial z}+\frac{V_r V_\theta}{r}=-\frac{1}{\rho r}\left(\frac{\partial p}{\partial \theta}\right)+\nu\left\{\frac{1}{r}\frac{\partial}{\partial r}\left(r\frac{\partial V_\theta}{\partial r}\right)+\frac{1}{r^2}\frac{\partial^2 V_\theta}{\partial \theta^2}+\frac{\partial^2 V_\theta}{\partial z^2}-\frac{V_\theta}{r^2}-\frac{2}{r^2}\frac{\partial V_r}{\partial \theta}\right\}+f_\theta \quad (3)$$

Momentum, z-direction:

$$V_r\frac{\partial V_z}{\partial r}+\frac{V_\theta}{r}\frac{\partial V_z}{\partial \theta}+V_z\frac{\partial V_z}{\partial z}=-\frac{1}{\rho}\left(\frac{\partial p}{\partial z}\right)+\nu\left\{\frac{1}{r}\frac{\partial}{\partial r}\left(r\frac{\partial V_z}{\partial r}\right)+\frac{1}{r^2}\frac{\partial^2 V_z}{\partial \theta^2}+\frac{\partial^2 V_r}{\partial z^2}\right\}+f_z \quad (4)$$

The following assumptions allow to simplify the above equations:

a) Steady, laminar flow;

b) The viscous force is treated as a body force acting on the flow at each (r - θ) position;

c) Two-dimensional flow:
   - ✓ $V_z = 0$;
   - ✓ V_r = constant across the channel
   - ✓ V_θ = constant across the channel

d) Radial symmetric flow field, uniform at the inlet ($r = r_0$). The flow field is thus the same for any θ, therefore the derivative $\frac{\partial}{\partial \theta} = 0$ for all flow variables;

e) $\left(\frac{\partial p}{\partial \theta}\right)$ negligible compared to wall friction forces.

2.2 Simplified Flow Equations

Taking into account the previous assumptions, the Navier-Stokes equations are reduced to:

Continuity:

$$\frac{1}{r}\frac{\partial(r\rho V_r)}{\partial r}=0 \quad (5)$$

Momentum, r-direction:

$$V_r\frac{\partial V_r}{\partial r}-\frac{{V_\theta}^2}{r}=-\frac{1}{\rho}\left(\frac{\partial p}{\partial r}\right)+f_r \quad (6)$$

Momentum, θ-direction:

$$V_r\frac{\partial V_\theta}{\partial r}+\frac{V_r V_\theta}{r}=f_\theta \quad (7)$$

Momentum, z-direction:

$$-\frac{1}{\rho}\left(\frac{\partial p}{\partial z}\right)=0 \quad (8)$$

The integration of the reduced continuity equation (5) results in $r\rho V_r = costant$. Furthermore, knowing the mass flow rate inside each channel, it follows that locally:

$$V_r=-\frac{\dot{m}_c}{2\pi r b \rho} \quad (9)$$

2.3 Formulation of the viscous shear stress

Considering a fluid element between the two disks defining the flow channel, a control volume V_e can be defined with base surface A_e and height b. The area wetted by the fluid A_w is $A_w = 2A_e$. Therefore, the hydraulic diameter D_h for the channel can be expressed as:

$$D_h = \frac{4[2\pi(r-r_i)b]}{[2\pi(r-r_i)2]} = 2b \qquad \rightarrow \quad b = \frac{D_h}{2} \tag{10}$$

Consequently,

$$A_e = \frac{Qe}{b} = \frac{2Qe}{D_h} \qquad A_w = 2A_e = \frac{4Qe}{D_h} \tag{11}$$

For laminar flow, the wall shear effect can be expressed as a function of a friction factor ζ and of the relative velocity of the flow. Equation (12) displays the expression of the wall shear stress, decomposing the relative velocity in its two components.

$$\tau_w = \frac{\zeta\rho}{2} w^2 = \frac{\zeta\rho}{2}\left[(V_\theta - \omega r)^2 + {V_r}^2\right] \tag{12}$$

Considering $U = \left({U_0}/{r_0}\right) r$ and $\zeta = {24}/{Re}$ as usual for laminar flow between parallel plates:

$$\zeta = \frac{24\mu}{\rho W D_h} = \frac{24\mu}{\rho W D_h} = \frac{24\mu}{\rho D_h \sqrt{(V_\theta - \omega r)^2 + {V_r}^2}} \tag{13}$$

So that:

$$\tau_w = \frac{\rho}{2}\frac{24\mu}{\rho D_h \sqrt{(V_\theta - \omega r)^2 + {V_r}^2}}\left[(V_\theta - \omega r)^2 + {V_r}^2\right] = \frac{12\mu}{D_h}\sqrt{(V_\theta - \omega r)^2 + {V_r}^2} \tag{15}$$

The force resulting from wall friction force is given by the product of the wall shear with the wetted area:

$$F = \tau_w A_w = \frac{48\mu Ve}{(D_h)^2}\sqrt{(V_\theta - \omega r)^2 + {V_r}^2} = \frac{12\mu Ve}{b^2}\sqrt{(V_\theta - \omega r)^2 + {V_r}^2} \tag{16}$$

The wall friction force has a tangential and a radial component, which influence respectively the torque and the radial pressure gradient.

2.4 Solution of the rotor flow

Figure 2 shows the local velocity triangle of the fluid element inside the rotor.

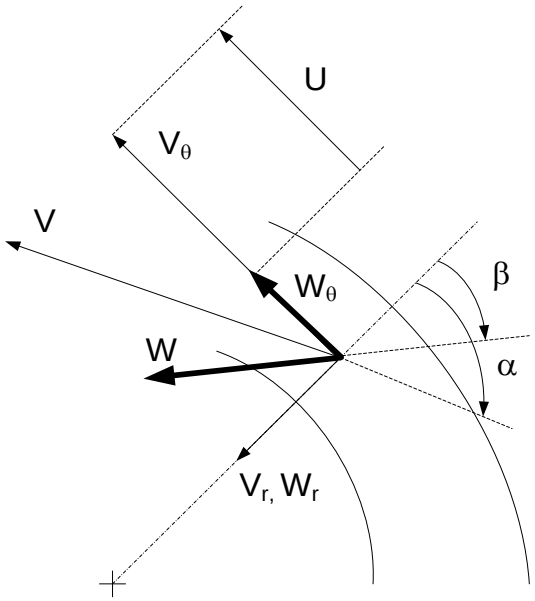

Fig. 2 – Local velocity triangle

The radial component of the force is given by:

$$F_r = F\cos(\beta) \tag{17}$$

Where β is the angle between relative velocity and the radial direction. Consequently $\cos(\beta)$ can be defined as:

$$\cos(\beta) = \frac{w_r}{w} = \frac{V_r}{\sqrt{(V_\theta - \omega r)^2 + {V_r}^2}} \tag{18}$$

Substituting (18) in (17), a compact expression of the radial force is obtained:

$$F_r = \frac{12\mu Ve\sqrt{(V_\theta - \omega r)^2 + {V_r}^2}}{b^2} \cdot \frac{V_r}{\sqrt{(V_\theta - \omega r)^2 + {V_r}^2}} = \frac{12\mu Ve}{b^2} V_r \tag{19}$$

Dividing (19) by the mass of the fluid element between two disks, the body force term in the radial direction can be expressed as:

$$f_r = \frac{12\mu}{\rho b^2} V_r \tag{20}$$

Proceeding in the same way for the tangential direction, the wall friction term is given by:

$$F_\theta = -F\sin(\beta) \tag{21}$$

$$\sin(\beta) = \frac{w_\theta}{w} = \frac{(V_\theta - \omega r)}{\sqrt{(V_\theta - \omega r)^2 + {V_r}^2}} \tag{22}$$

Similarly, substituting (22) in (21), a compact expression of the tangential force is obtained:

$$F_\theta = -\frac{12\mu Ve\sqrt{(V_\theta - \omega r)^2 + {V_r}^2}}{b^2}\frac{(V_\theta - \omega r)}{\sqrt{(V_\theta - \omega r)^2 + {V_r}^2}} = -\frac{12\mu Ve}{b^2}(V_\theta - \omega r) \quad (23)$$

So that the body force term in tangential direction can be obtained:

$$f_\theta = -\frac{3\mu}{\rho b^2}(V_\theta - \omega r) \quad (24)$$

In order to determine the local pressure, (20) is substituted in (6):

$$V_r\frac{\partial V_r}{\partial r} - \frac{{V_\theta}^2}{r} = -\frac{1}{\rho}\left(\frac{\partial p}{\partial r}\right) + \frac{12\mu}{\rho b^2}V_r \quad (25)$$

Using (9), the local derivative $\frac{\partial V_r}{\partial r}$ can be expressed as:

$$\frac{\partial V_r}{\partial r} = \frac{\dot{m}_c}{2\pi r^2 b\rho} = -\frac{1}{r} * \left(-\frac{\dot{m}_c}{2\pi r b\rho}\right) = -\frac{1}{r}V_r \quad (26)$$

Finally, substituting (26) in (25) the pressure gradient in radial direction is given by:

$$\left(\frac{\partial p}{\partial r}\right) = -\frac{12\mu}{b^2}\left(\frac{\dot{m}_c}{2\pi r b\rho}\right) + \frac{\rho}{r}\left(\frac{\dot{m}_c}{2\pi r b\rho}\right)^2 + \frac{\rho}{r}{V_\theta}^2 \quad (27)$$

Likewise, in order to define the tangential velocity, (24) can be substituted in (7):

$$V_r\frac{\partial V_\theta}{\partial r} + \frac{V_r V_\theta}{r} = -\frac{12\mu}{\rho b^2}(V_\theta - \omega r) \quad (28)$$

Obtaining finally:

$$\frac{\partial V_\theta}{\partial r} = \frac{24\mu\pi r(V_\theta - \omega r)}{b\dot{m}_c} - \frac{V_\theta}{r} \quad (29)$$

Which determines the profile of $V_\theta(r)$.

2.5 Flow Model Results - Validation

Equations (27) and (29) were programmed into a one-dimensional (r-direction) EES [18] code with a second-order finite difference approximation. In order to validate the model, it was decided to run the simulations for the same data documented in [3] and for incompressible fluid (ρ = constant).

Table 1. Documented data from [3] and [7]

Fluid	Air
Inlet Rotor Total Temperature	368 K
Inlet Rotor Total Pressure	101 kPa
Mass flow rate	0.00194 kg/s
Inlet Rotor Diameter	0.1778 m
Revolution per minute	6300 RPM

The trends of pressure, tangential and radial velocity of the fluid for variable radius can be observed in Figure 3. The radial velocity increases decreasing the radius of the turbine, according to (9). The tangential velocity profile is determined by two main effects: the conservation of angular

momentum (which tends to increase the velocity of the fluid), and viscous forces (which conversely tend to decrease fluid velocity). At high x_i values, viscous forces are predominant, whereas the conservation of angular momentum prevails at low x_i values.

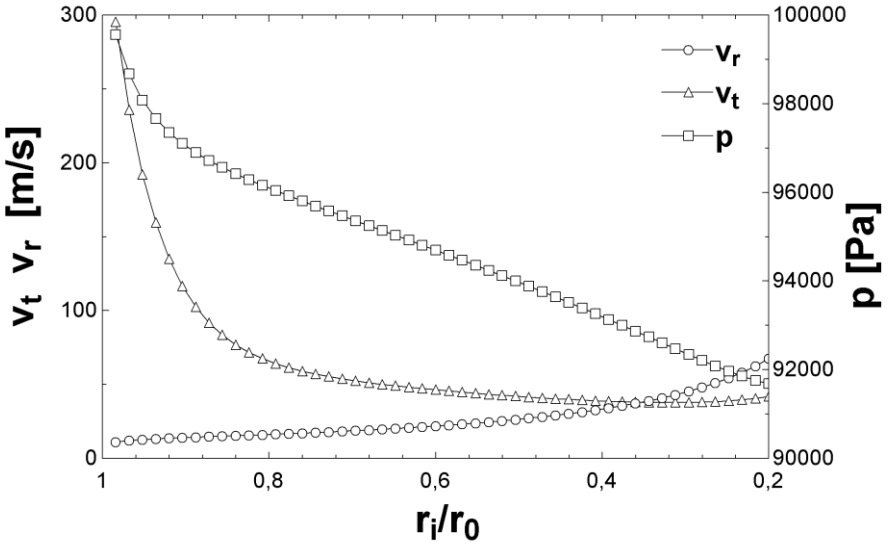

Fig.3 Pressure, tangential and radial velocity components versus non-dimensional radius

Figure 4 shows a comparison of the model results (relative tangential component of velocity) with the analytical formulations proposed in [7] and [9]. The results are coincident with the velocities calculated in [7]. The solution reported in [9] is slightly different: this is due to some different assumptions. In particular, the model reported in [9] considers a viscous flow, rather than introducing equivalent body forces along r and θ directions (simplifying hypothesis (b), assumed here and in [7]).

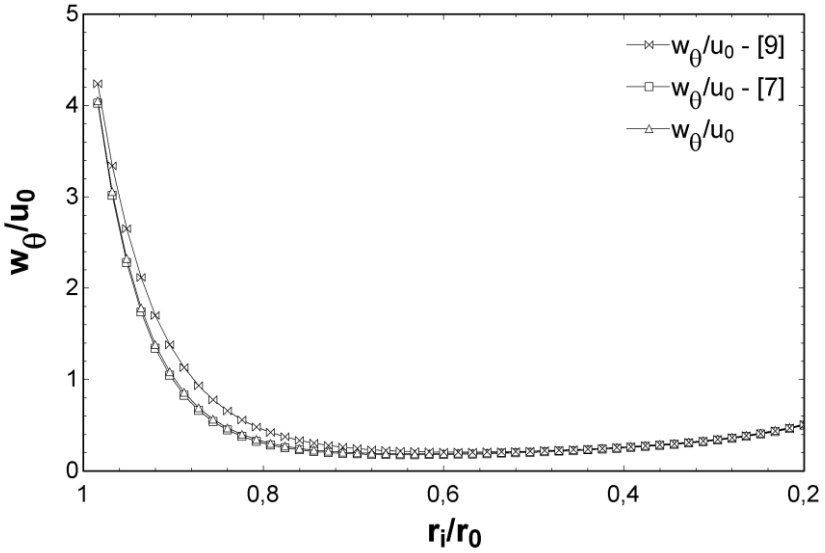

Fig. 4 Comparison between model and literature; tangential component of relative velocity

3 Performance of the Tesla turbine rotor

3.1 Performance indicators

In order to assess the performance potential of the turbine, a parametric study needs to be performed. The parametric analysis should show the performance as a function of the main design variables, which are non-dimensionalized following common practice in turbomachinery [19]. All the results obtained in the parametric analysis refer to air as the working fluid.

The flow and load coefficient can be expressed as:

$$\phi = \frac{v_{r0}}{U_0} \tag{30}$$

$$\psi = \frac{work}{\frac{U_0^2}{2}} = \frac{V_{\theta 0}U_0 - V_{\theta 1}U_1}{\frac{U_0^2}{2}} \tag{31}$$

The specific speed and the non-dimensional specific diameter are given by:

$$N_s = rpm * \frac{\left(\frac{\dot{m}}{\rho_0}\right)^{0.5}}{\left((h_0 - h_1) + \frac{v_0^2}{2}\right)^{0.75}} \tag{32}$$

$$D_s = D_0 * \frac{\left(\frac{(h_0 - h_1) + \frac{v_0^2}{2}}{g}\right)^{0.25}}{\left(\frac{\dot{m}_c}{\rho_0}\right)^{0.5}} \tag{33}$$

The total-to-static efficiency of the turbine is defined as:

$$\eta = \frac{work}{\Delta h_{0s}} = \frac{V_{\theta 0}U_0 - V_{\theta 1}U_1}{(h_0 - h_1) + \frac{v_0^2}{2}} \tag{34}$$

Moreover, critical design parameters for the Tesla turbine were identified in the geometrical ratios (D_1/D_0) and (b_0/D_0); for output conditions the exit kinetic energy and the absolute flow angle, which should be as low as possible were identified as critical performance indicators. The exit kinetic energy is presented in non-dimensionalized form as:

$$\xi_1 = \frac{E_{kin,1}}{\Delta h_{0s}} = \frac{\frac{v_1^2}{2}}{(h_0 - h_1) + \frac{v_0^2}{2}} \tag{35}$$

And the exit fluid angle can be calculated as:

$$\alpha = \tan^{-1}\left(\frac{v_{\theta 1}}{v_{r1}}\right) \tag{36}$$

3.2 Overall performance results

The trend of the rotor efficiency as a function of (D_1/D_0) and (b_0/D_0) is shown in Figure 5.

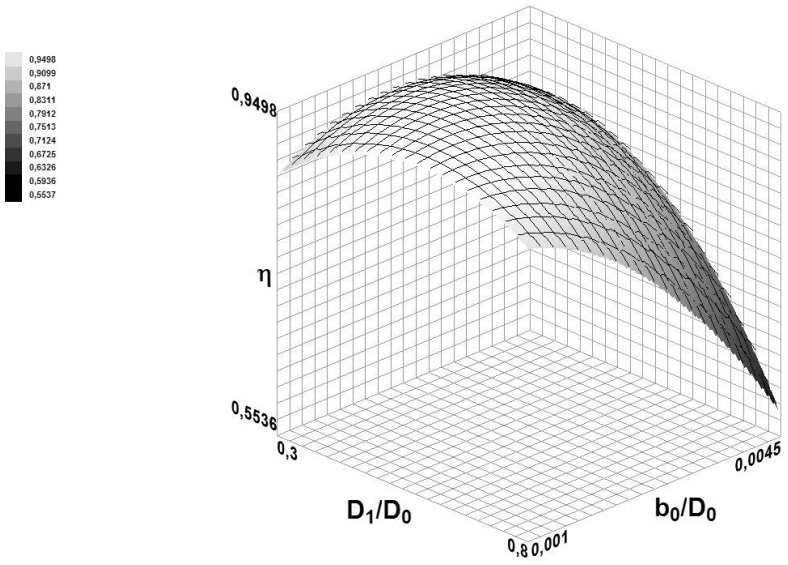

Fig. 5 Rotor Efficiency η vs D_1/D_0 and b_0/D_0

The rotor efficiency is only slightly affected by different values of the exit diameter. With decreasing D_1/D_0, the larger kinetic energy at discharge, due to the higher axial component of velocity, appears to be somewhat compensated by the larger rotor surface available for momentum exchange between the fluid and the disks.

On the other hand, the (b_0/D_0) parameter - the non-dimensional gap between two disks - strongly affects the efficiency of the rotor. This is due to the influence of the Reynolds number in the laminar flow regime, which can be best explained re-arranging its definition and remembering that $b = \frac{D_h}{2}$:

$$Re = \frac{\rho * v_r * D_h}{\mu} = \frac{\dot{m}_c}{2\pi r b \rho} * \frac{\rho * D_h}{\mu} = \frac{\dot{m}_c}{\pi r \rho} \quad (37)$$

Similarly, the trend of the load coefficient Ψ versus (D_1/D_0) and (b_0/D_0) is shown in Figure 6. Ψ is very sensitive to the reduction of (b_0/D_0); however – differently from rotor efficiency η- it also shows a sensitivity to (D_1/D_0). The momentum exchange is favoured as the wet area is increased; nevertheless, the exit diameter should not exceed a certain limit, the penalty being an increase of the residual tangential velocity, leading to higher discharge losses. On the whole, values of $0,35 < (D_1/D_0) < 0,45$ and $0,005 < (b_0/D_0) < 0,015$ appear recommendable.

An important parameter, which is strongly influenced by the gap between disks, is the absolute exit angle (Figure 7). In order to reduce it and render possible an efficient recovery of discharge kinetic energy, the exit fluid angle should be close to axial ($\alpha_1 \cong 0$). A reduction of the gap between the plates is definitely beneficial to this end. The decrease of α for smaller values of b_0 is due to the reduction of the tangential component, as well as to the increase in the radial component of absolute velocity. The reduction of tangential velocity, as can be noted from (29), is due to the increase of viscous momentum transfer for small values of b_0. On the other hand, the radial velocity increases because of the continuity (9).

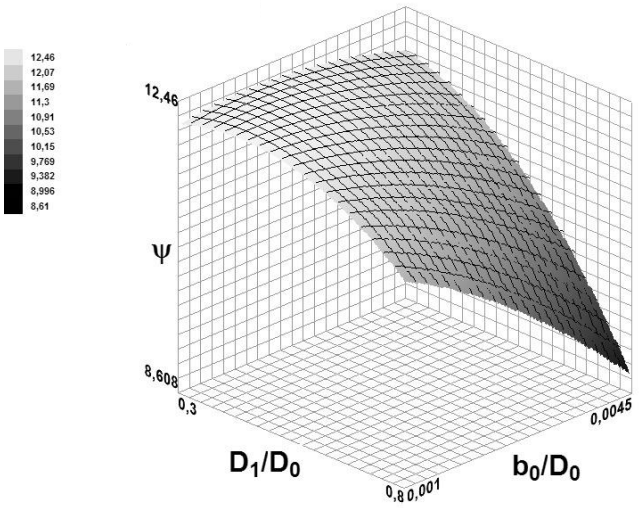

Fig. 6 Rotor Load Coefficient Ψ vs D_1/D_0 and b_0/D_0

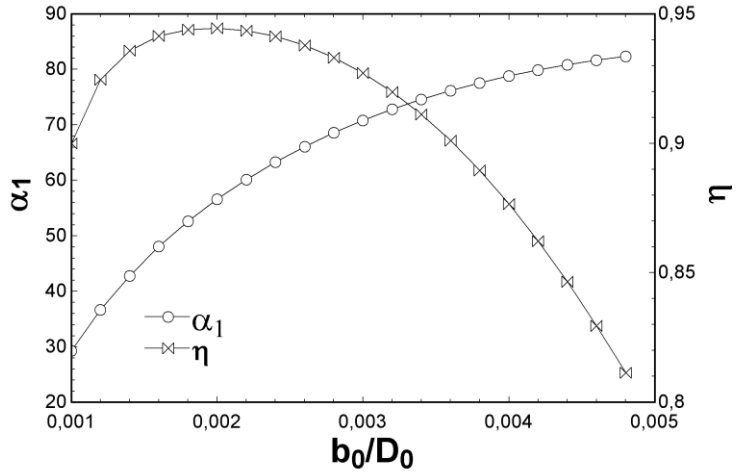

Fig. 7 Exit fluid angle α and efficiency of the turbine vs b_0/D_0, for D_1/D_0 = 0.44

The trend of the absolute velocity and of its components with variable gap is displayed in figure 8. The modulus of velocity results from the combination of the radial and tangential components. The absolute exit velocity has a minimum, determined by opposite trends with b_0/D_0 of the two components of velocity (radial and tangential). The minimum of the exit kinetic energy E_{kin1} corresponds to maximization of the rotor efficiency.

As for the influence of the flow coefficient, the absolute exit angle and the efficiency are plotted against Φ in figure 9. Increasing flow coefficient values, the absolute exit angle decreases. This is due to an increase of the radial component of the fluid, which therefore turns the fluid in the axial direction. If values of exit flow angles below 50° are sought, then a flow coefficient in the range Φ = 0,2 should be selected; under these conditions, the rotor efficiency is still high – in the range of 0,94.

It is interesting to calculate N_s and D_s ((32) and (33)); the resulting placement of an optimized Tesla rotor on Balje's diagram is shown in Figure 10. It can be seen that the performance of the Tesla rotor exceeds in its N_s – D_s range that of competing expanders (notably, rotary piston expanders or drag turbines).

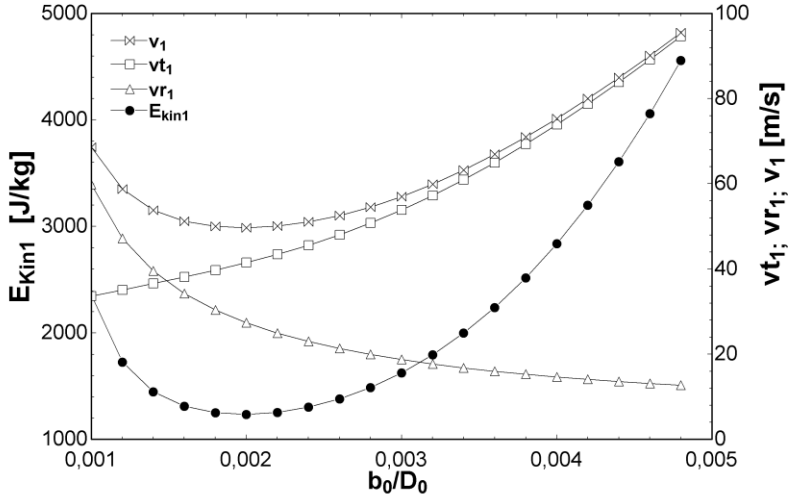

Fig. 8 Exit kinetic energy vs non dimensional gap

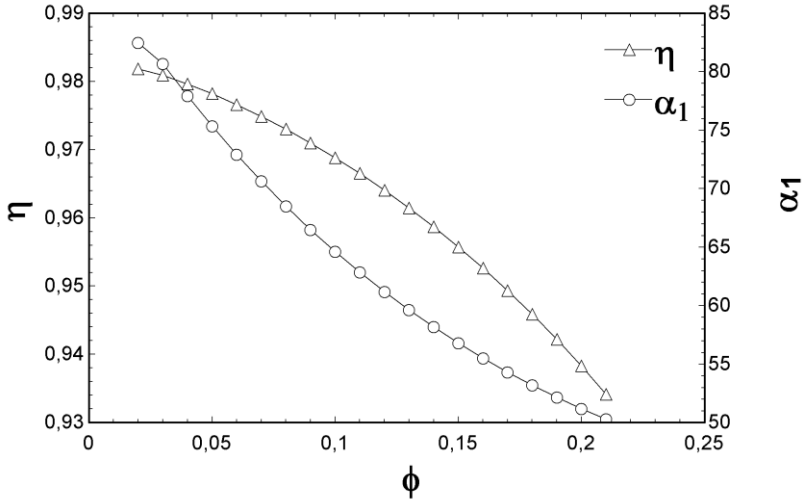

Fig.9 α_1 and η versus Φ

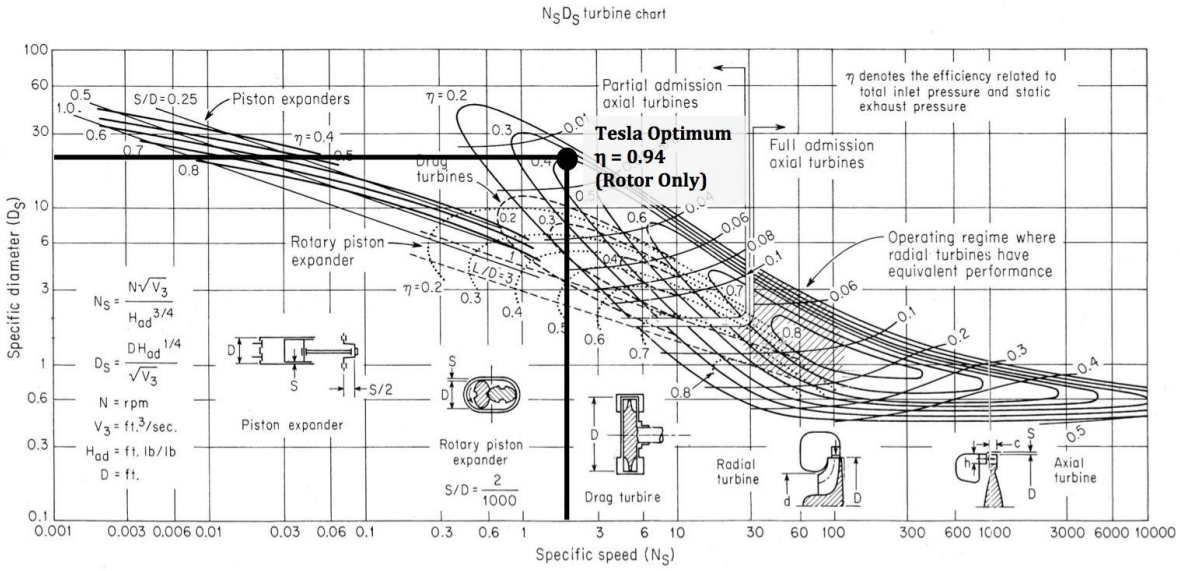

Fig.10 The Tesla rotor on the Balje diagram

The final geometry is summarized in table 2.

Table 2. Final geometry of Tesla rotor (working fluid = air)

Mass flow rate $\dot{m}_c$	0.00194 [kg/s]
Rotational speed	6300 [RPM]
Inlet Mach number	1
Inlet Diameter D_0	0.1778 [m]
Exit Diameter D_1	0.0772 [m]
Gap b_0	0.00032 [m]
Absolut exit angle α_1	52 [°]
Power produced for each channel	40.8 [W]
Exit Mach number	0.1168
Specific Speed, N_s	2.057 [RPM·ft$^{3/4}$·s$^{-1/2}$]
Specific Diameter, D_s	20.69 [ft$^{-1/4}$·s$^{1/2}$]

4 Conclusions

An upgraded description of the Tesla turbine rotor flow was presented and validated against similar literature models. The new model has the advantage of considering variable density and to be easily adaptable to non-conventional fluids. Existing experience with prototypes of Tesla turbines have always been developed with air or steam as working fluid, so that the capability of dealing with general fluids looks potentially attractive.

The model was applied to evaluate the sensitivity of performance to the most relevant design variables, that is: D_1/D_0; b_0/D_0; and the flow coefficient. The calculated performance parameters are efficiency and the work coefficient; moreover, non-dimensional variables suitable for comparison to expanders of different type (N_s and D_s) were calculated.

The results indicate that the Tesla rotor appears potentially competitive with other expander designs, with special reference to the expander efficiency.

These results certainly need further development, with special reference to the calculation of nozzle flow and to the evaluation of other relevant losses (leakage, heat transfer, …). Future works will explore different working fluids, applying the Tesla turbine concept to small Organic Rankine Cycles.

Nomenclature

A	surface, m^2
b	gap between two discs, m
D_h	hydraulic diameter, m
D_s	specific diameter, ft$^{-1/4}$·s$^{1/2}$
f	body force per unit mass, m/s^2
E	kinetic energy, J/kg
F	force, N
h	enthalpy, J/kg

$\dot{m}$	mass flow rate, kg/s
N_s	specific speed, RPM·ft$^{3/4}$·s$^{-1/2}$
p	pressure, Pa
Q	volume, m^3
r	local radius, m
Re	Reynolds number (relative flow)
rpm	rotational speed, rpm
T	temperature, °C
U	tangential velocity, m/s
V	absolute velocity, m/s
x	non-dimensional radius
w	Relative velocity, m/s
$\dot{W}$	power, W

Greek symbols

α	absolute flow angle, °
β	relative flow angle, °
ζ	friction factor
η	total-to-static efficiency (rotor only)
μ	dynamic viscosity, kg/(ms)
ν	kinematic viscosity, m^2/s
ξ	non-dimensionalized kinetic energy
ρ	density, kg/m^3
τ	wall shear stress, Pa
Φ	flow coefficient
Ψ	load coefficient
ω	rotational speed, rad/s

Subscripts and superscripts

0	rotor inlet value
1	rotor outlet value
e	fluid element
i	point i
kin	kinetic
r	radial direction
t	time, s
w	wetted wall
z	axial direction
θ	tangential direction

References

[1] Tesla, N., (1913), "Turbine", U.S. Patent No. 1 061 206.

[2] Armstrong, J.H., (1952), "An Investigation of the Performance of a Modified Tesla Turbine", M.S. Thesis, Georgia Institute of Technology.

[3] Rice, W., (1965); "An analytical and experimental investigation of multiple-disk turbines", *ASME Journal of Engineering for Power,* Vol. 87, Issue 1, pp. 29-36.

[4] Hoya, G.P. and Guha, A., (2009), "The design of a test rig and study of the performance and efficiency of a Tesla disc turbine", *Proceedings of the Institution of Mechanical Engineers, Part A: Journal of Power and Energy,* Vol. 223.

[5] Guha, A., and Smiley, B., (2009), "Experiment and analysis for an improved design of the inlet and nozzle in Tesla disc turbines", *Proceedings of the Institution of Mechanical Engineers, Part A: Journal of Power and Energy,* Vol. 224, pp. 261-277. DOI: 10.1243/09576509JPE818

[6] Neckel A.L., and Godinho, M., (2015), "Influence of geometry on the efficiency of convergent-divergent nozzles applied to Tesla turbines", *Experimental Thermal and Fluid Science,* Vol. 62, pp. 131-140.

[7] Carey, V.P., (2010), "Assessment of Tesla Turbine Performance for Small Scale Rankine Combined Heat and Power Systems", *Journal of Eng. for Gas Turbines and Power,* Vol. 132.

[8] Carey, V.P., (2010), "Computational/Theoretical Modeling of Flow Physics and Transport in Disk Rotor Drag Turbine Expanders for Green Energy Conversion Technologies", *Proceedings of the ASME 2010 International Mechanical Engineering Congress and Exposition*, Vol. 11, pp. 31-38. DOI:10.1115/IMECE2010-41017

[9] Guha, A., and Sengupta S., (2013), "The fluid dynamics of the rotating flow in a Tesla disc turbine", *European Journal of Mechanics B/Fluids,* Vol. 37, pp. 112-123.

[10] Sengupta, S., and Guha, A., (2012), "A theory of Tesla disc turbines", *Proceedings of the Institution of Mechanical Engineers, Part A; Journal of Power and Energy*. DOI: 10.1177/0957650912446402

[11] Lemma, E., Deam, R.T., Toncich, D., Collins, R., (2008), "Characterisation of a small viscous flow turbine", *Experimental Thermal and Fluid Science,* Vol. 33, pp. 96-105.

[12] Sengupta, S. and Guha A., (2013), "Analytical and computational solutions for three-dimensional flow-field and relative pathlines for the rotating flow in a Tesla disc turbine", *Computers & Fluids*, Vol. 88, pp. 344-353

[13] Romanin, V.D., Krishnan, V.G., Carey, V.P., Maharbiz, M.M., (2012), "Experimental and Analytical study of Sub-Watt Scale Tesla Turbine Performance", in: *Proceedings of the ASME 2012 International Mechanical Engineering Congress & Exposition,* Vol. 7, pp. 1005-1014. DOI:10.1115/IMECE2012-89675

[14] Krishnan, V.G., Romanin, V.D., Carey, V.P., Maharbiz, M.M., (2013), "Design and scaling of microscale Tesla turbines", *Journal of Micromechanics and Microengineering,* Vol. 23, Issue 12. DOI: 10.1088/0960-1317/23/12/125001

[15] Guha, A., and Sengupta S., (2014), "Similitude and scaling laws for the rotating flow between concentric discs", *Proceedings of the Institution of Mechanical Engineers, Part A; Journal of Power and Energy,* Vol. 28, pp. 429-439. DOI: 10.1177/0957650914523947

[16] Guha, A., and Sengupta S., (2014), "The fluid dynamics of work transfer in the non-uniform viscous rotating flow within a Tesla disc turbomachine", *Physics of Fluids,* Vol. 26, Issue 3. DOI: 10.1063/1.4866263

[17] Sengupta, S. and Guha A., (2016), "Flow of a nanofluid in the microspacing within co-rotating discs of a Tesla turbine", *Applied Mathematical Modelling,* Vol. 40, Issue 1, pp. 485-499. DOI: 10.1016/j.apm.2015.05.012

[18] Klein, S.A. and Nellis, G.F., (2012), "Mastering EES", *f-Chart software*

[19] Dixon, S., L., (2005), *Fluid Mechanics and Thermodynamics of Turbomachinery,* 5th ed., Pergamon Press.